Modern Physics Letters A
Vol. 28, No. 23 (2013) 1350105 (14 pages)

DOI: 10.1142/S0217732313501058





# THE STUDY OF QCD PHASE TRANSITION AT FINITE TEMPERATURE AND CHIRAL CHEMICAL POTENTIAL IN A DYSON–SCHWINGER EQUATION MODEL

LIU-JUN LUO*, SONG SHI* and HONG-SHI ZONG*,†

*Department of Physics, Nanjing University, Nanjing Jiangsu 210093, P. R. China
†Joint Center for Particle, Nuclear Physics and Cosmology, Nanjing 210093, P. R. China
†State Key Laboratory of Theoretical Physics, Institute of Theoretical Physics, CAS, Beijing 100190, P. R. China
†zonghs@chenwang.nju.edu.cn

Received 9 June 2013
Accepted 17 June 2013
Published 15 July 2013

In this paper, we use a separable gluon propagator model to study the Quantum Chromodynamics (QCD) phase transition at finite temperature and chiral chemical potential. Using this model, we calculate the quark condensate and the chiral susceptibility at finite temperature and chiral chemical potential both in the chiral limit and at finite current quark mass. Based on these, we obtain the QCD phase diagram in the $\mu_5 - T$ plane.

*Keywords*: Chiral phase transition; deconfinement; PNJL model.

PACS Nos.: 12.38.Mh, 12.39.-x, 12.38.Lg

## 1. Introduction

The phase transition of Quantum Chromodynamics (QCD) is one of the most important and interesting aspects of the physics of strongly interacting matter. There have been many works dedicated to search the phase transition line at RHIC and LHC. In Ref. 1, the authors use numerical simulations to study the QCD phase transition at zero baryonic chemical potential and finite temperature. In Refs. 2–5, the authors use the Dyson-Schwinger Equation (DSE) method to study the chiral phase transition in QCD. In the literatures, the Taylor expansion method[6] and the density of state method[7] are used to study the phase diagram of QCD. In Refs. 8 and 9, it was considered that the topological charge fluctuations in the gauge configuration may be induced by thermal fluctuations. The chiral magnetic effect was

†Corresponding author

studied in Refs. 10–15. The presence of the axial charge has profound consequences on meson physics and it has been studied in Ref. 16.

From Refs. 10–16, we can see that the chiral chemical potential plays an important role. In this paper, using a separable gluon propagator model in the framework of DSE approach, we give a first attempt to study the effect of chiral chemical potential on the QCD phase transition. In Sec. 2, we derive the gap equation at finite temperature and finite baryonic and chiral chemical potential in the separable gluon propagator model. In Sec. 3, the expressions of quark condensate and chiral susceptibility in the separable gluon propagator model are derived. In Sec. 4, the numerical results for quark condensate and chiral susceptibility are analyzed. Based on these, the QCD phase diagram in the $\mu_5 - T$ plane is obtained. A summary and outlook is given in Sec. 5.

## 2. The Gap Equation at Finite Temperature and Chiral Chemical Potential

In the study of QCD phase transition at finite temperature and finite chemical potential, the rainbow DSE and ladder BSE is a commonly adopted approach.[17] In this paper, we will employ a separable gluon propagator model[18] to study the QCD phase transition at finite temperature and chiral chemical potential. At finite $T$ and baryonic chemical potential $\mu$, the quark propagator can be written as

$$G^{-1}(\widetilde{p_n}) = i\widetilde{\not{p}_n}A_n + B_n\,, \tag{1}$$

where $\widetilde{p_n} = (\mathbf{p}, \widetilde{p_{4n}}) = (\mathbf{p}, p_{4n} + i\mu)$ with $p_{4n} = \pi T(2n+1)$. The quark gap equation at finite $T$ and baryonic chemical potential $\mu$ in the separable gluon propagator model reads (we employ the Euclidean metric in this paper):

$$G^{-1}(\widetilde{p_n}) = i\widetilde{\not{p}_n} + m_0 + \frac{4T}{3}\sum_l \int \frac{d^3\mathbf{q}}{(2\pi)^3} D_0 f_0(p_n) f_0(q_l)\gamma_\mu G(\widetilde{q_l})\gamma_\mu\,, \tag{2}$$

where $m_0$ is the current quark mass and the function $f_0(p_n)$ is defined as:

$$f_0(p_n) = \exp\left(-\frac{p_n^2}{\Lambda_0^2}\right) = \exp\left(-\frac{\mathbf{p}^2 + p_{4n}^2}{\Lambda_0^2}\right) \tag{3}$$

with the parameters $\Lambda_0 = 687$ MeV and $D_0\Lambda_0^2 = 128$.

In the study of the chiral magnetic effect, one needs to introduce a chiral chemical potential $\mu_5$ coupled to the chiral density operator $\bar{\psi}\gamma_4\gamma_5\psi$, and we add a new term $\mu_5\bar{\psi}\gamma_4\gamma_5\psi$ into the Lagrangian. At finite $T$ and finite baryonic and chiral chemical potential, the quark propagator can be written as

$$G^{-1}(\widetilde{p_n}, \mu_5) = i\widetilde{\not{p}_n}A_n + B_n - C_n\mu_5\gamma_4\gamma_5\,. \tag{4}$$

The quark gap equation at finite $T$ and finite baryonic and chiral chemical potential in the separable gluon propagator model reads:

$$G^{-1}(\widetilde{p_n},\mu_5) = i\widetilde{\not{p}_n} + m_0 - \mu_5\gamma_4\gamma_5 + \frac{4T}{3}\sum_l \int \frac{d^3\mathbf{q}}{(2\pi)^3} D_0 f_0(p_n) f_0(q_l)\gamma_\mu G(\widetilde{q_l},\mu_5)\gamma_\mu \,. \tag{5}$$

From Eqs. (4) and (5), we can obtain

$$A_n = 1 + \frac{\widetilde{p_{4n}}}{\widetilde{p_n^2}} f_0(p_n) a(T,\mu,\mu_5)\,, \tag{6}$$

$$B_n = m_0 + f_0(p_n) b(T,\mu,\mu_5)\,, \tag{7}$$

$$C_n\mu_5 = \mu_5 - f_0(p_n) c(T,\mu,\mu_5)\,, \tag{8}$$

where the functions $a$, $b$ and $c$ satisfy the following coupled integral equations:

$$a(T,\mu,\mu_5) = \frac{4T}{3\pi^2}\sum_l \int dq\, q^2 D_0 f_0(q_l) \frac{A_l \widetilde{q_{4l}}(B_l^2 + A_l^2\widetilde{q_l}^2 + C_l^2\mu_5^2)}{(B_l^2 + A_l^2\widetilde{q_l}^2 + C_l^2\mu_5^2)^2 - 4A_l^2C_l^2\mu_5^2 q^2}\,, \tag{9}$$

$$b(T,\mu,\mu_5) = \frac{8T}{3\pi^2}\sum_l \int dq\, q^2 D_0 f_0(q_l) \frac{B_l(B_l^2 + A_l^2\widetilde{q_l}^2 + C_l^2\mu_5^2)}{(B_l^2 + A_l^2\widetilde{q_l}^2 + C_l^2\mu_5^2)^2 - 4A_l^2C_l^2\mu_5^2 q^2}\,, \tag{10}$$

$$c(T,\mu,\mu_5) = \frac{4T}{3\pi^2}\sum_l \int dq\, q^2 D_0 f_0(q_l) \frac{C_l\mu_5(B_l^2 + A_l^2(\widetilde{q_{4l}^2} - \mathbf{q}^2) + C_l^2\mu_5^2)}{(B_l^2 + A_l^2\widetilde{q_l}^2 + C_l^2\mu_5^2)^2 - 4A_l^2C_l^2\mu_5^2 q^2}\,. \tag{11}$$

Equations (9)–(11) are the analytic form of the gap equation in the separable gluon propagator model. The DSE approach is based on path integral formalism and we can compare this method to other models such as the PNJL model.[19–22]

## 3. The Quark Condensate and Chiral Susceptibility at Finite Temperature and Finite Chiral Chemical Potential

The quark condensate at finite $T$ and $\mu_5$ can be written as

$$-\langle\bar{\Psi}\Psi\rangle = N_c N_f T \sum_l \int \frac{d^3q}{(2\pi)^3}\,\mathrm{tr}(G(q,\mu_5)\,, \tag{12}$$

where $N_c$ and $N_f$ are the number of colors and flavors, respectively (in this paper, we take $N_c = 3$ and $N_f = 2$). The chiral susceptibility is defined as

$$\chi = \frac{\partial(-\langle\bar{\Psi}\Psi\rangle)}{\partial m_0}\,. \tag{13}$$

Substituting Eq. (5) into Eqs. (12) and (13), we obtain

$$-\langle\bar{\Psi}\Psi\rangle = \frac{12T}{\pi^2}\sum_l \int dq\, q^2 \frac{B_l(B_l^2 + A_l^2\widetilde{q}^2 + C_l^2\mu_5^2)}{(B_l^2 + A_l^2\widetilde{q}^2 + C_l^2\mu_5^2)^2 - 4A_l^2C_l^2\mu_5^2 q^2}\,, \tag{14}$$

$$\chi = \frac{12T}{\pi^2}\sum_l \int dq\, q^2 \Bigg( \frac{\frac{\partial B_l}{\partial m_0}(B_l^2 + A_l^2\widetilde{q}^2 + C_l^2\mu_5^2)}{(B_l^2 + A_l^2\widetilde{q}^2 + C_l^2\mu_5^2)^2 - 4A_l^2C_l^2\mu_5^2q^2}$$

$$+ \frac{2B_l\big(B_l\frac{\partial B_l}{\partial m_0} + \widetilde{q}^2A_l\frac{\partial A_l}{\partial m_0} + C_l\mu_5\frac{\partial(C_l\mu_5)}{\partial m_0}\big)}{(B_l^2 + A_l^2\widetilde{q}^2 + C_l^2\mu_5^2)^2 - 4A_l^2C_l^2\mu_5^2q^2}\Bigg)$$

$$- \frac{12T}{\pi^2}\sum_l \int dq\, q^2 4B_l(B_l^2 + A_l^2\widetilde{q}^2 + C_l^2\mu_5^2)\Bigg[(B_l^2 + A_l^2\widetilde{q}^2 + C_l^2\mu_5^2)$$

$$\times\left(B_l\frac{\partial B_l}{\partial m_0} + \widetilde{q}^2A_l\frac{\partial A_l}{\partial m_0} + C_l\mu_5\frac{\partial(C_l\mu_5)}{\partial m_0}\right) - 2q^2\Bigg(A_l\frac{\partial A_l}{\partial m_0}C_l^2\mu_5^2$$

$$+ A_l^2C_l\mu_5\frac{\partial(C_l\mu_5)}{\partial m_0}\Bigg)\Bigg]\Bigg/\Big[(B_l^2 + A_l^2\widetilde{q}^2 + C_l^2\mu_5^2)^2 - 4A_l^2C_l^2\mu_5^2q^2\Big]^2 . \quad (15)$$

The expressions for the partial derivatives $\frac{\partial A_n}{\partial m_0}$, $\frac{\partial B_n}{\partial m_0}$ and $\frac{\partial C_n\gamma_5}{\partial m_0}$ will be given in Appendix A. The free quark propagator at finite $T$ and finite baryonic and chiral chemical potential is

$$G^{-1}(\widetilde{p_n}, \mu_5) = i\widetilde{\not{p}_n} + m_0 - \mu_5\gamma_4\gamma_5 . \quad (16)$$

Substituting Eq. (16) into Eqs. (12) and (13), we can obtain the expression for the free chiral susceptibility

$$\chi_{\text{free}} = \frac{12T}{\pi^2}\sum_l \int dq\, q^2 \Bigg[\frac{(3m_0^2 + \tilde{q}^2 + \mu_5^2)}{(m_0^2 + \tilde{q}^2 + \mu_5^2)^2 - 4\mu_5^2q^2}$$

$$- 4\frac{m_0^2(m_0^2 + \tilde{q}^2 + \mu_5^2)^2}{((m_0^2 + \tilde{q}^2 + \mu_5^2)^2 - 4\mu_5^2q^2)^2}\Bigg]. \quad (17)$$

## 4. Analysis of the Numerical Results and the QCD Phase Diagram in the $\mu_5 - T$ Plane

By numerically solving the gap equations (9)–(11), one can obtain the quark propagator. From this, one can calculate the quark condensate and chiral susceptibility at finite $T$ and $\mu_5$. The numerical results are shown below. Here, all the results are obtained at $\mu = 0$.

Figure 1 shows the $T$-dependence of $\mathrm{Re}\, b(T, \mu, \mu_5)$ for $\mu = 0$ and different $\mu_5$ in the chiral limit. From this figure, we can see that for a fixed chiral chemical potential $\mu_5$, the real part of $b(T, \mu, \mu_5)$ falls off to zero at high enough temperature. As $\mu_5$ increases, the critical temperature at which $\mathrm{Re}\, b$ vanishes increases slightly at first, and then decreases when $\mu_5$ is large enough. This shows that the chiral chemical potential can strongly affect the $T$-dependence of quark condensate in the chiral limit.

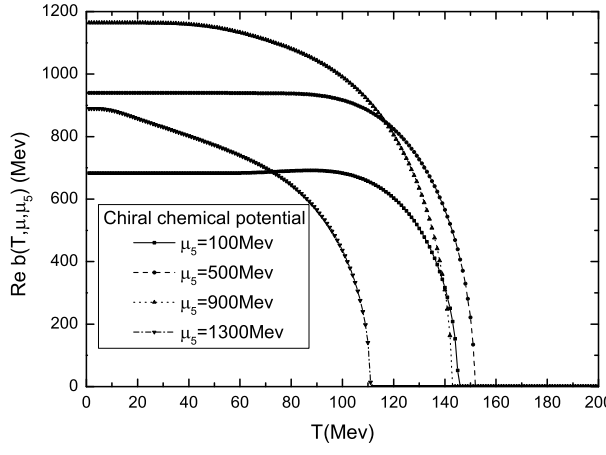


Fig. 1. The $T$-dependence of $\mathrm{Re}\, b(T, \mu, \mu_5)$ for $\mu = 0$ and different $\mu_5$ in the chiral limit.

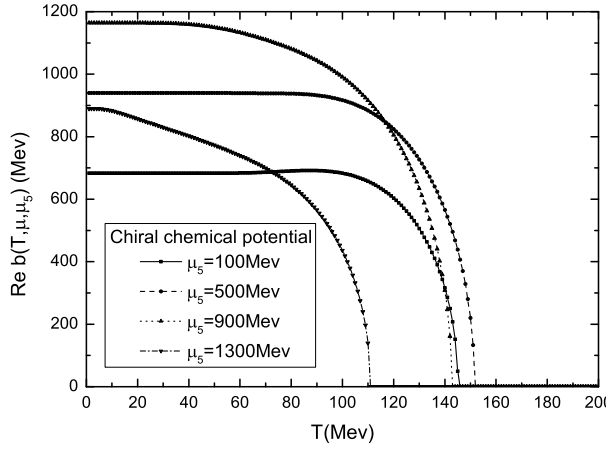


Fig. 2. The $T$-dependence $\mathrm{Re}\, b(T, \mu, \mu_5)$ for $\mu = 0$ and different $\mu_5$ at $m_0 = 5.5$ MeV.

Figure 2 shows the $T$-dependence of $\mathrm{Re}\, b$ for $m_0 = 5.5$ MeV. Comparing Fig. 2 with Fig. 1, we can see that when the current quark mass increases to a nonzero value, the behavior of $\mathrm{Re}\, b$ with the variation of temperature does not change. As $\mu_5$ increases, the critical temperature increases at first and then decreases. As the current quark mass increases, the value of $\mathrm{Re}\, b$ changes slightly from its value in the chiral limit at relatively small temperatures.

Figure 3 shows the $T$-dependence of the real part of quark condensate for different $\mu_5$ for both the chiral limit case and the case of $m_0 = 5.5$ MeV. From Fig. 3(a), we can see that the behavior of the quark condensate in the chiral limit accords with that of $\mathrm{Re}\, b$. For fixed value of $\mu_5$, the quark condensate vanishes at some critical temperature. With the increase of $\mu_5$, the critical temperature increases at first and

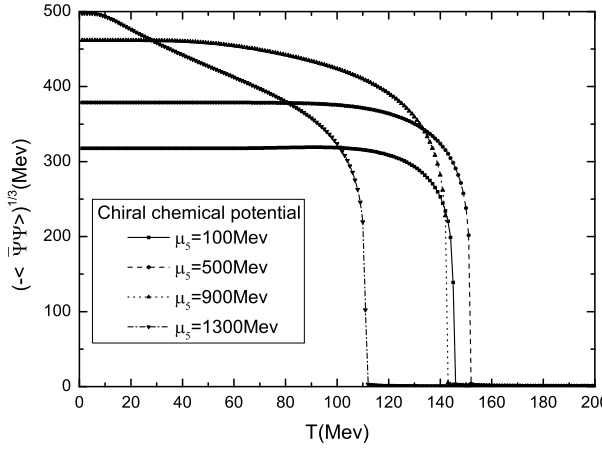


(a)

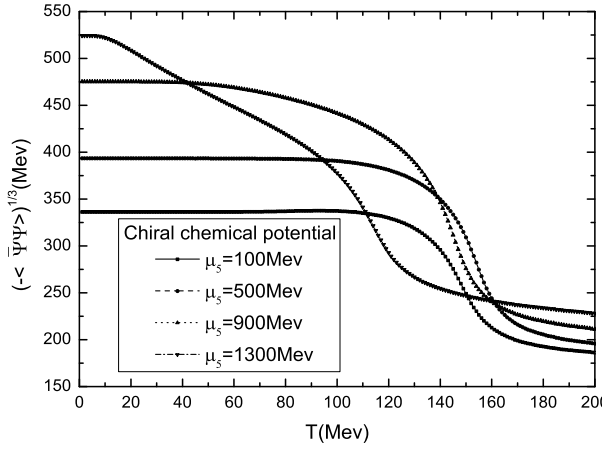


(b)

Fig. 3. The $T$-dependence of quark condensate for $\mu = 0$ and different $\mu_5$. (a) The chiral limit case. (b) $m_0 = 5.5$ MeV.

then decreases. When $\mu_5 = 1520$ MeV, the quark condensate almost equals to zero in the whole temperature range we study.

From Fig. 3(b), it can be seen that the chiral condensate at $m_0 = 5.5$ MeV has similar $T$-dependence as that in the chiral limit. The quark condensate decreases quickly at large temperature but does not go to zero as in the chiral limit case. As $\mu_5$ increases, the region in the temperature axis in which the quark condensate decreases at first shifts to right and then shifts to left.

Since the quark condensate drops from a big value to nearly zero when the phase transition occurs, we can use it as an order parameter to determine the phase transition line in the $\mu_5 - T$ plane in the chiral limit. For all values of $\mu_5$ the quark

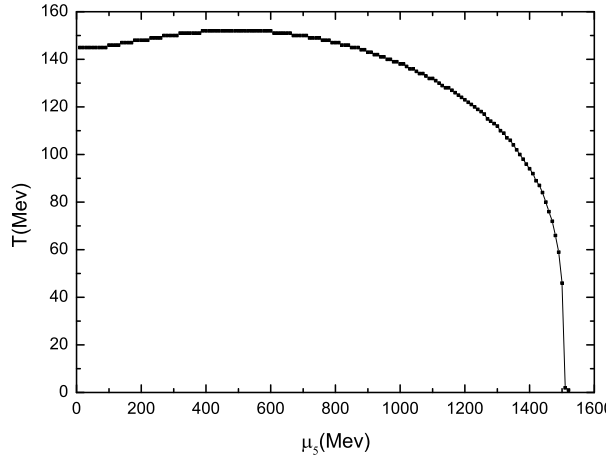


Fig. 4. The phase transition line at $\mu = 0$ in the chiral limit determined using the quark condensate as the order parameter. This phase transition is of first-order because the quark condensate drops to zero at the phase transition point.



condensate drops from a big value to zero as $T$ increases. At $\mu_{5c} = 1520$ MeV the quark condensate almost equals to zero in the whole temperature range we study. Therefore, from the behavior of the quark condensate, we conclude that the phase transition is of first-order. From Fig. 4, it can be seen that the critical temperature at $\mu_5 = 0$ is $T_c = 145$ MeV and the critical chiral chemical potential at $T_c = 0$ is $\mu_{5c} = 1520$ MeV. In Ref. 22, the authors obtained $T_c \simeq 190$ MeV when the constituent quark mass $M = 339$ MeV at $eB = 0$. Below the phase transition line, the quark condensate is nonzero and the system is in the baryon phase, while above the phase transition line, the quark condensate vanishes and the system is in a phase where chiral symmetry is partially restored. As $\mu_5$ increases from zero, the phase transition temperature increases to a maximum 152 MeV and then decreases monotonously until it vanishes at $\mu_5 = \mu_{5c}$.

We can also use the chiral susceptibility as the order parameter to determine the phase transition line in the $\mu_5 - T$ plane. The $T$-dependence of the chiral susceptibility for different current quark mass at $\mu = 0$ and $\mu_5 = 0$ is shown in Fig. 5. From Fig. 5, it can be seen that for different current quark mass the chiral susceptibility shows a peak at some temperature. The peak for the chiral limit case is much higher than the one at finite current quark mass and it can be considered as a divergence. So, from the behavior of chiral susceptibility we conclude that the phase transition is of second-order in the chiral limit. When the current quark mass is finite, the chiral susceptibility is continuous. In this case, we have a crossover. From this figure, we can see that our results for the chiral susceptibility at $\mu = \mu_5 = 0$ for different current quark mass are similar to that in Ref. 3. This shows that adding a chiral chemical potential in the DSE model is feasible. The phase transition temperature for different current quark mass is listed in Table 1.

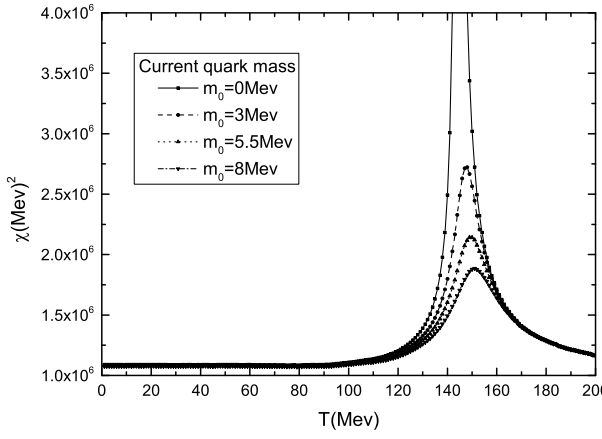


Fig. 5. The $T$-dependence of the real part of the chiral susceptibility for different current quark mass at $\mu = 0$ and $\mu_5 = 0$.

Table 1. The phase transition temperature for different current quark mass.

| Type | $m_0$ (MeV) | $T$ (MeV) |
|---|---|---|
| 2nd | 0 | 145 |
| crossover | 3 | 148 |
| crossover | 5.5 | 149 |
| crossover | 8 | 151 |

From Table 1 and Fig. 5, it can be seen that as the current quark mass increases, the phase transition temperature increases and the peak of the chiral susceptibility decreases.

In order to understand the phase transition at finite temperature and chiral chemical potential in more detail, we show the $T$-dependence of the chiral susceptibility and its value normalized by the free chiral susceptibility in the chiral limit in Fig. 6. From Fig. 6(a), we can see that for different $\mu_5$ the chiral susceptibility is divergent at some temperature. Therefore, from the behavior of the chiral susceptibility we conclude that the phase transition is of second-order. Its behavior is similar to that of Re $b$ in Fig. 1. As the chiral chemical potential increases, the temperature at which the chiral susceptibility diverges increases at first and then decreases. From Fig. 6(b), we can see that the normalized susceptibility approaches to one at large temperature, as is expected in advance.

In order to see how the current quark mass affects the phase transition line in the $\mu_5 - T$ plane, we show the $T$-dependence of the real part of chiral susceptibility for $\mu = 0$ and different $\mu_5$ at $m_0 = 5.5$ MeV in Fig. 7. From Fig. 7, it can be seen that for different $\mu_5$ the chiral susceptibility shows similar behavior as the one in

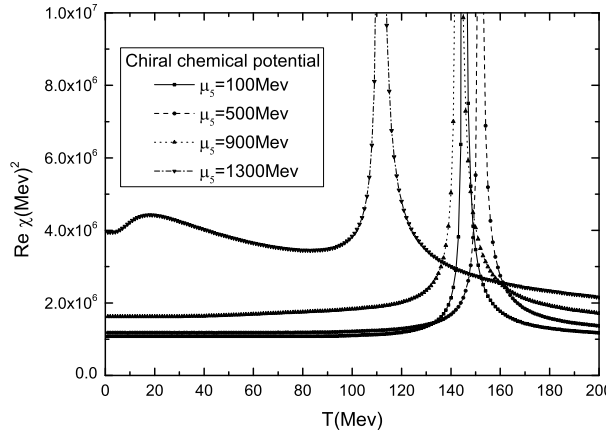


(a)

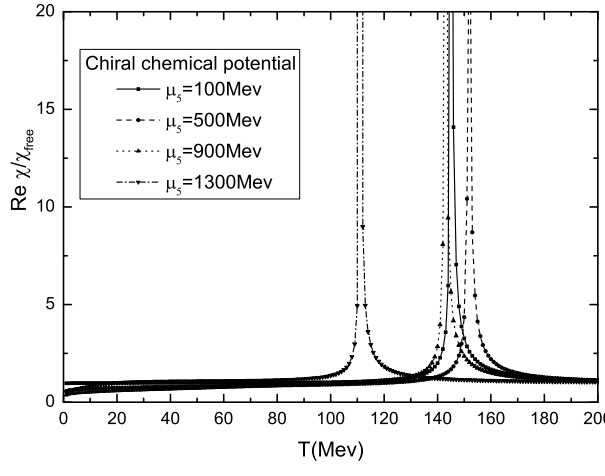


(b)

Fig. 6. The $T$-dependence of the real part of the chiral susceptibility for $\mu = 0$ and different $\mu_5$ in the chiral limit. (a) The $T$-dependence of the real part of the chiral susceptibility. (b) The $T$-dependence of the real part of the chiral susceptibility normalized by the free chiral susceptibility.

the chiral limit, but the susceptibility shows a finite peak instead of a divergence at some temperature. Therefore, in the case of finite current quark mass we have a crossover.

From the calculated results of the chiral susceptibility, we obtain the phase transition line in the $\mu_5 - T$ plane for both the chiral limit case and the case of $m_0 = 5.5$ MeV and it is shown in Fig. 8. The lower line in Fig. 8 stands for the second-order phase transition line in the chiral limit, and its location is the same as the first-order phase transition line as determined using the quark condensate as the order parameter. We see that different order parameter will give different

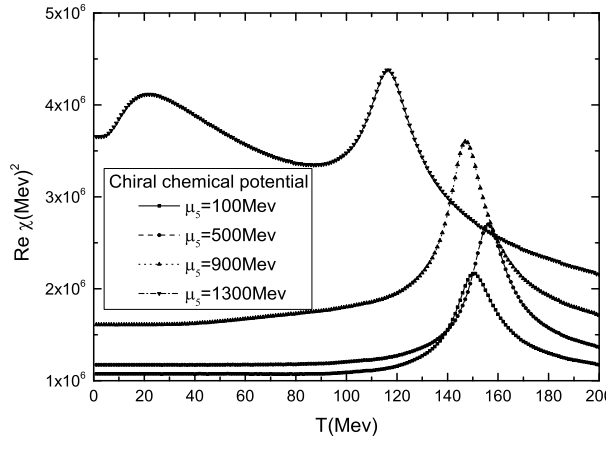


(a)

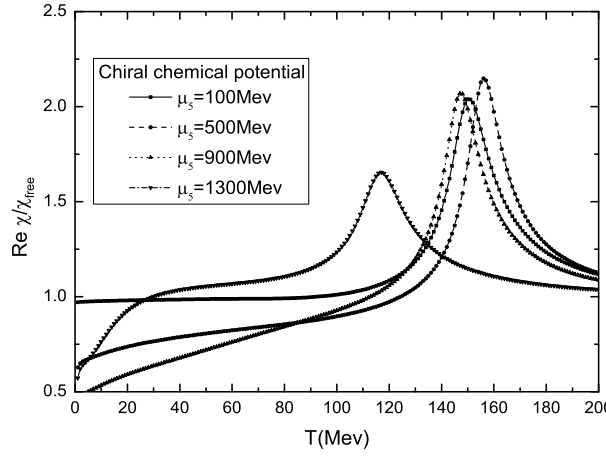


(b)

Fig. 7. The $T$-dependence of the real part of the chiral susceptibility for $\mu = 0$ and different $\mu_5$ at $m_0 = 5.5$ MeV. (a) The $T$-dependence of the real part of the chiral susceptibility. (b) The $T$-dependence of the real part of the chiral susceptibility normalized by the free chiral susceptibility.

results on the type of phase transition, but the location of the phase transition line is independent of which order parameter we choose.

The upper line in Fig. 8 stands for the crossover at $m_0 = 5.5$ MeV. It can be seen that the critical temperature at $\mu_5 = 0$ is $T_c = 149$ MeV and the critical chiral chemical potential at $T_c = 0$ is $\mu_{5c} = 1560$ MeV. In Ref. 20, the author obtained $T_c = 174.1$ MeV using the quark-meson model, and obtained $T_c = 173.9$ MeV for $m_q = 5.5$ MeV using PNJL model, which is bigger than our results. We conclude that as the current quark mass increases, for a given value of $\mu_5$ (or $T$), the corresponding phase transition point in the $T$ (or $\mu_5$) axis increases, too.

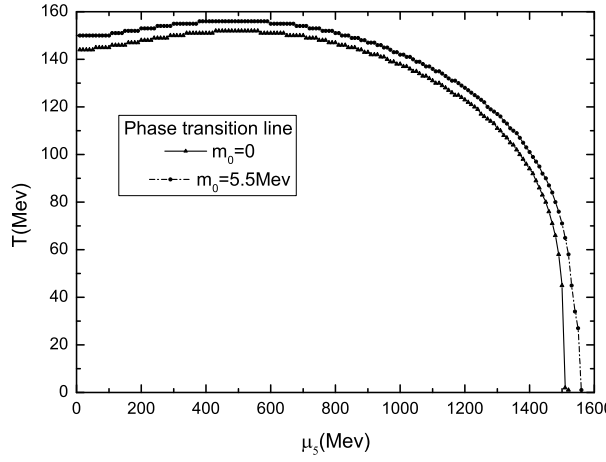


Fig. 8. The phase transition line in the $\mu_5 - T$ plane at zero baryonic chemical potential for different current quark mass. The lower one is the second-order phase transition line in the chiral limit, and the upper one is the crossover at $m_0 = 5.5$ MeV.

In Table 2, we list the value of the critical temperature $T_c$, the critical chiral chemical potential $\mu_{5c}$ and the maximal temperature $T_{\max}$ in the phase transition line for both the chiral limit case and the case of $m_0 = 5.5$ MeV.

Table 2. $T_c$, $\mu_{5c}$ and the maximal temperature $T_{\max}$ for both the chiral limit case and the case of $m_0 = 5.5$ MeV.

| Type | $m_0$ (MeV) | $T_c$ (MeV) | $T_{\max}$ (MeV) | $\mu_{5c}$ (MeV) |
|---|---|---|---|---|
| 2nd | 0 | 145 | 152 | 1520 |
| crossover | 5.5 | 149 | 156 | 1560 |

## 5. Summary and Outlook

In this paper, we study the QCD phase transition at finite temperature and chiral chemical potential using a separable gluon propagator model in the framework of the DSE approach. Using the quark condensate as the order parameter, we obtain $T_c = 145$ MeV in the chiral limit, and using the chiral susceptibility as the order parameter, we obtain $T_c = 149$ MeV at $m_0 = 5.5$ MeV. The $T_c$ increases as the current quark mass increases, and approaches the value of $T_c$ in Ref. 22. Moreover, using the chiral susceptibility as the order parameter, we find that in the chiral limit the phase transition is of second-order, whereas at finite current quark mass ($m_0 = 5.5$ MeV) it is a crossover. Both the critical temperature $T_c$ and the critical chiral chemical potential $\mu_{5c}$ increase as the current quark mass increases. In our model, as $\mu_5$ increases, the critical temperature increases slightly at first, then drops until it vanishes at $\mu_5 = \mu_{5c}$, which is different from the results obtained in Refs. 19 and 20 that the critical temperature decreases monotonously as $\mu_5$ increases.

The DSE provides a successful description for various non-perturbative aspects of strong interaction physics, and it is a useful tool to study the QCD phase transition at finite temperature and chiral chemical potential just as other methods.[19–22] So, we expect that we can use the method in this paper to furtherly study the topological charge and chiral magnetic effect in the near future.

## Appendix A

In this Appendix, we give the expressions for the partial derivatives $\frac{\partial A_n}{\partial m_0}$, $\frac{\partial B_n}{\partial m_0}$ and $\frac{\partial C_n\gamma_5}{\partial m_0}$.

$$\frac{\partial A_n}{\partial m_0} = \frac{\widetilde{p_{4n}}}{\widetilde{p^2}} f_0(p) \frac{\partial(a(T,\mu,\mu_5))}{\partial m_0}\,, \tag{A.1}$$

$$\frac{\partial B_n}{\partial m_0} = 1 + f_0(p) \frac{\partial(b(T,\mu,\mu_5))}{\partial m_0}\,, \tag{A.2}$$

$$\frac{\partial(C_n\mu_5)}{\partial m_0} = -f_0(p) \frac{\partial(c(T,\mu,\mu_5))}{\partial m_0}\,, \tag{A.3}$$

$$\begin{aligned}
&\frac{\partial(a(T,\mu,\mu_5))}{\partial m_0} \\
&= \frac{4T}{3\pi^2}\sum_l \int dq\, q^2 D_0 f_0(q) \bigg[\frac{\partial A_l}{\partial m_0}\widetilde{q_{4l}}(B_l^2 + A_l^2\tilde{q}^2 + C_l^2\mu_5^2) + 2A_l\widetilde{q_{4l}}\bigg(B_l\frac{\partial B_l}{\partial m_0} \\
&\quad + \tilde{q}^2 A_l\frac{\partial A_l}{\partial m_0} + C_l\mu_5\frac{\partial(C_l\mu_5)}{\partial m_0}\bigg)\bigg] \Big/ \Big[(B_l^2 + A_l^2\tilde{q}^2 + C_l^2\mu_5^2)^2 - 4A_l^2C_l^2\mu_5^2q^2\Big] \\
&\quad - \frac{4T}{3\pi^2}\sum_l \int dq\, q^2 D_0 f_0(q) 4A_l\widetilde{q_{4l}}(B_l^2 + A_l^2\tilde{q}^2 + C_l^2\mu_5^2)\bigg[(B_l^2 + A_l^2\tilde{q}^2 + C_l^2\mu_5^2) \\
&\quad \times \bigg(B_l\frac{\partial B_l}{\partial m_0} + \tilde{q}^2 A_l\frac{\partial A_l}{\partial m_0} + C_l\mu_5\frac{\partial(C_l\mu_5)}{\partial m_0}\bigg) - 2q^2\bigg(A_l\frac{\partial A_l}{\partial m_0}C_l^2\mu_5^2 \\
&\quad + A_l^2 C_l\mu_5\frac{\partial(C_l\mu_5)}{\partial m_0}\bigg)\bigg] \Big/ \Big[(B_l^2 + A_l^2\tilde{q}^2 + C_l^2\mu_5^2)^2 - 4A_l^2C_l^2\mu_5^2q^2\Big]^2\,,
\end{aligned} \tag{A.4}$$

$$\begin{aligned}
&\frac{\partial(b(T,\mu,\mu_5))}{\partial m_0} \\
&= \frac{8T}{3\pi^2}\sum_l \int dq\, q^2 D_0 f_0(q) \bigg[\frac{\partial B_l}{\partial m_0}(B_l^2 + A_l^2\tilde{q}^2 + C_l^2\mu_5^2) + 2B_l\bigg(B_l\frac{\partial B_l}{\partial m_0} \\
&\quad + \tilde{q}^2 A_l\frac{\partial A_l}{\partial m_0} + C_l\mu_5\frac{\partial(C_l\mu_5)}{\partial m_0}\bigg)\bigg] \Big/ \Big[(B_l^2 + A_l^2\tilde{q}^2 + C_l^2\mu_5^2)^2 - 4A_l^2C_l^2\mu_5^2q^2\Big]
\end{aligned}$$

$$-\frac{8T}{3\pi^2}\sum_l\int dq\,q^2D_0f_0(q)4B_l(B_l^2+A_l^2\tilde{q}^2+C_l^2\mu_5^2)\Big[(B_l^2+A_l^2\tilde{q}^2+C_l^2\mu_5^2)$$
$$\times\left(B_l\frac{\partial B_l}{\partial m_0}+\tilde{q}^2A_l\frac{\partial A_l}{\partial m_0}+C_l\mu_5\frac{\partial(C_l\mu_5)}{\partial m_0}\right)-2q^2\Big(A_l\frac{\partial A_l}{\partial m_0}C_l^2\mu_5^2$$
$$+A_l^2C_l\mu_5\frac{\partial(C_l\mu_5)}{\partial m_0}\Big)\Big]\Big/\Big[(B_l^2+A_l^2\tilde{q}^2+C_l^2\mu_5^2)^2-4A_l^2C_l^2\mu_5^2q^2\Big]^2, \qquad (A.5)$$

$$\frac{\partial(c(T,\mu,\mu_5))}{\partial m_0}$$
$$=\frac{4T}{3\pi^2}\sum_l\int dq\,q^2D_0f_0(q)\Big[\frac{\partial(C_l\mu_5)}{\partial m_0}(B_l^2+A_l^2({\tilde{q_0}}^2-q^2)+C_l^2\mu_5^2)+2C_l\mu_5$$
$$\times\left(B_l\frac{\partial B_l}{\partial m_0}+({\tilde{q_0}}^2-q^2)A_l\frac{\partial A_l}{\partial m_0}+C_l\mu_5\frac{\partial(C_l\mu_5)}{\partial m_0}\right)\Big]\Big/\Big[(B_l^2+A_l^2\tilde{q}^2+C_l^2\mu_5^2)^2$$
$$-4A_l^2C_l^2\mu_5^2q^2\Big]-\frac{4T}{3\pi^2}\sum_l\int dq\,q^2D_0f_0(q)4C_l\mu_5(B_l^2+A_l^2({\tilde{q_0}}^2-q^2)+C_l^2\mu_5^2)$$
$$\times\Big[(B_l^2+A_l^2\tilde{q}^2+C_l^2\mu_5^2)\Big(B_l\frac{\partial B_l}{\partial m_0}+\tilde{q}^2A_l\frac{\partial A_l}{\partial m_0}+C_l\mu_5\frac{\partial(C_l\mu_5)}{\partial m_0}\Big)$$
$$-2q^2\left(A_l\frac{\partial A_l}{\partial m_0}C_l^2\mu_5^2+A_l^2C_l\mu_5\frac{\partial(C_l\mu_5)}{\partial m_0}\right)\Big]\Big/\Big[(B_l^2+A_l^2\tilde{q}^2+C_l^2\mu_5^2)^2$$
$$-4A_l^2C_l^2\mu_5^2q^2\Big]^2. \qquad (A.6)$$



## Acknowledgment

This work is supported in part by the National Natural Science Foundation of China (under Grant Nos. 11275097, 10935001 and 11075075) and the Research Fund for the Doctoral Program of Higher Education (under Grant No. 2012009111002).

## References

1. Y. Aoki, Z. Fodor, S. D. Katz and K. K. Szabo, *Phys. Lett. B* **643**, 46 (2006).
2. M. He, D. K. He, H. T. Feng, W. M. Sun and H. S. Zong, *Phys. Rev. D* **76**, 076005 (2007).
3. M. He, F. Hu, W. M. Sun and H. S. Zong, *Phys. Lett. B* **675**, 32 (2009).
4. B. Wang, W. M. Sun and H. S. Zong, *Mod. Phys. Lett. A* **28**, 1350064 (2013).
5. Y. Jiang, H. Chen, W. M. Sun and H. S. Zong, *JHEP* **04**, 014 (2013).
6. C. R. Allton *et al.*, *Phys. Rev. D* **71**, 054508 (2005).
7. J. Ambjorn, K. N. Anagnostopoulos, J. Nishimura and J. J. M. Verbaarschot, *JHEP* **10**, 062 (2002).
8. A. M. Polyakov, *Nucl. Phys. B* **120**, 429 (1977).
9. D. Kharzeev and A. Zhitnitsky, *Nucl. Phys. A* **797**, 67 (2007).

10. D. Kharzeev, R. D. Pisarski and M. H. G. Tytgat, *Phys. Rev. Lett.* **81**, 512 (1998).
11. D. Kharzeev, *Phys. Lett. B* **633**, 260 (2006).
12. D. Kharzeev, *Ann. Phys.* (*N. Y.*) **325**, 205 (2010).
13. D. E. Kharzeev, L. D. McLerran and H. J. Warringa, *Nucl. Phys. A* **803**, 227 (2008).
14. K. Fukushima, D. E. Kharzeev and H. J. Warringa, *Phys. Rev. D* **78**, 074033 (2008).
15. K. Fukushima, D. E. Kharzeev and H. J. Warringa, *Nucl. Phys. A* **836**, 311 (2010).
16. A. A. Andrianov, D. Espriu and X. Planells, arXiv:1210.7712v1.
17. C. D. Roberts and A. G. Williams, *Prog. Part. Nucl. Phys.* **33**, 477 (1994).
18. D. Blaschke and G. Burau, *Int. J. Mod. Phys. A* **16**, 2267 (2001).
19. R. Gatto and M. Ruggieri, *Phys. Rev. D* **85**, 054013 (2012).
20. M. Ruggieri, *Phys. Rev. D* **84**, 014011 (2011).
21. M. N. Chernodub and A. S. Nedelin, *Phys. Rev. D* **83**, 105008 (2011).
22. K. Fukushima, M. Ruggieri and R. Gatto, *Phys. Rev. D* **81**, 114031 (2010).